This is the Pre-Published Version.

This is the peer reviewed version of the following article: Yin, M. J., Zhang, Y., Yin, Z., Zheng, Q., & Zhang, A. P. (2018). Micropatterned Elastic Gold‐Nanowire/Polyacrylamide Composite Hydrogels for Wearable Pressure Sensors. Advanced Materials Technologies, 3(7), 1800051, which has been published in final form at https://doi.org/10.1002/admt.201800051. This article may be used for non-commercial purposes in accordance with Wiley Terms and Conditions for Use of Self-Archived Versions.

Article type: Full Paper

Micropatterned Elastic Gold-Nanowire/Polyacrylamide Composite Hydrogels for Wearable Pressure Sensors

*Ming-jie Yin, Yangxi Zhang, Zhigang Yin, Qingdong Zheng, and A. Ping Zhang**

Dr. M.-J. Yin, Dr. Y. Zhang, Prof. A. P. Zhang

Photonics Research Center, Department of Electrical Engineering, The Hong Kong Polytechnic University, Hong Kong SAR, China

E-mail: azhang@polyu.edu.hk

Dr. Z. Yin, Prof. Q. Zheng

State Key Laboratory of Structural Chemistry, Fujian Institute of Research on the Structure of Matter, Chinese Academy of Sciences, 155 Yangqiao West Road, Fuzhou, China.

Keywords: elastic hydrogels, supramolecular, photopolymerization, pressure sensors, wearable devices

Abstract:

Elastic hydrogels have recently attracted remarkable attention because of their unique mechanical and stimulus-responsive properties. In this work, we develop a novel elastic supramolecular hydrogel for wearable pressure sensors by photocrosslinking polyacrylamide (PAAm) through covalent bonds and hydrogen bonds as well as ionic bonds in the presence of poly(acrylic acid) and Ca^{2+}. Gold nanowires (Au NWs) were homogeneously mingled with the PAAm hydrogel to attain a conductive composite hydrogel. Using an in-house optical maskless exposure technology, printable piezoresistive pressure sensors were quickly fabricated by directly patterning the composite hydrogel into micro-ribs on flexible electrodes. The pressure sensors with micro-rib structures exhibited a bimodal contact mode between Au NWs, which provided a new pathway to engineer the sensor's sensitivity and operation range. In the experiments, the pressure sensor with optimized micro-rib structures showed not only ultrahigh sensitivity (i.e. 3.71 kPa-1 in the pressure range of 0-2.8 kPa) but also low detection limit (i.e. 0.2 Pa) and long-term stability. A flexible hand-shape electrode device and an arterial pulse monitoring sensor have been demonstrated to reveal the potentials of such a pressure sensor on wearable device applications.

This article may not be enhanced, enriched or otherwise transformed into a derivative work, without express permission from Wiley or by statutory rights under applicable legislation. Copyright notices must not be removed, obscured or modified. The article must be linked to Wiley's version of record on Wiley Online Library and any embedding, framing or otherwise making available the article or pages thereof by third parties from platforms, services and websites other than Wiley Online Library must be prohibited.

1. Introduction

Flexible electronic devices, with the ability of transducing physical clues, such as pressure,[1] humidity,[2] strain,[3] and temperature[4] into electrical signals, have attained remarkable progress in recent years.[5] In particular, flexible pressure sensors have been paid dramatic attention to because of their broad applications in biomedical devices,[6] artificial intelligence,[7] wearable electronics,[1c, 8] and so on. For instance, organic thin-film transistor (OTFT)-based pressure sensors[1b, 1f, 9] have been demonstrated to measure human wrist pulses for personalized healthcare applications. However, the structures of OTFTs are relatively complex, which makes their fabrication process rigid and costly. Therefore, there is still enduring enthusiasm to develop new wearable pressure sensors to enhance their merits, such as high sensitivity, wide operation range, flexibility, economic fabrication and deployment costs.[7c]

Several mechanisms have been used to fabricate pressure sensors, such as piezoelectricity,[3a, 10] capacitance,[1b, 1f, 11] triboelectricity,[12] and piezoresistivity.[1c, 1e, 13] Among them, piezoresistivity-type pressure sensors have the advantages of simple structure, low-cost, and convenient read-out, and thus have been drawn incredible attention to the development of flexible devices. To sustain large deformation, this type of flexible pressure sensor is commonly fabricated by elastic polymer materials, such as polydimethylsiloxane (PDMS),[1c, 13a] polyurethane (PU),[1h] and even polypyrrole (PPy).[1d] Although such devices have shown their impressive performances, the sensitivities of those sensors are still not very high and/or their operation ranges are not wide enough for many applications.[8b] For example, the pressure sensor fabricated by Park et al.[1e] using Au-coated PDMS as the active matrix has a sensitivity of 2 kPa^{-1} under a pressure lower than 220 Pa. When the pressure increases above 220 Pa, its sensitivity starts to drop, and it will eventually reach saturation when the pressure reaches 3.5 kPa. Based on quantum tunneling effect, Lee et al.[1h] demonstrated a pressure sensor using a PU matrix mixed with sea-urchin shaped metal nanoparticles, and

improved the sensitivity to 2.46 kPa^{-1}. However, its high sensitivity can be achieved only when the pressure is lower than 1 kPa. It will decrease to 0.055 kPa^{-1} when the applied pressure is above 10 kPa.

One of the promising solutions to this issue is to adopt elastic hydrogels, which have significantly lower modulus of elasticity, for flexible pressure sensing applications. Using hollow-sphere microstructured PPy hydrogel, Bao's group[1d] achieved a remarkable leap of sensitivity to an unprecedently high level of 133.1 kPa^{-1}. However, the high sensitivity can only sustain at the pressure up to 30 Pa. It will decrease significantly to 0.05 kPa^{-1} when the pressure goes above 10 kPa. Therefore, a remaining challenge is how to develop flexible pressure sensors with both high sensitivity and wide operation range. This problem might be solved by using hydrogel with high stretchability and toughness. Suo's group[14] demonstrated a novel polyacrylamide (PAAm) composite hydrogel with excellent elasticity due to the double network formed by both covalent and ionic bonds. Based on the superior elastic property of PAAm composite hydrogels, Duan et al.[13b] demonstrated a pressure sensor using a PAAm-based conductive elastic hydrogel through polymerization of acrylamide and aniline in the swollen chitosan microspheres colloid. The sensor exhibits a very wide response range of 0.1 to 600 kPa. However, its sensitivity is not high, i.e. 0.35 and 0.03 kPa^{-1} in the pressure ranges of 0 - 1.5 and 1.5 - 10 kPa, respectively.

To achieve both high sensitivity and wide operation range, herein, we develop a flexible pressure sensor by using an elastic supramolecular hydrogel with micro-rib structures. A novel PAAm-based supramolecular hydrogel with three kinds of bonding forces, which make the hydrogel saliently elastic, was prepared through a controlled UV polymerization process. Gold nanowires (Au NWs) were mixed to make the elastic hydrogel conductive and suited to soft electronics.[15] Moreover, an optical maskless exposure technology was used to simultaneously control the crosslinking degree of the hydrogel and micropattern the hydrogel into micro-rib structures to regulate the hydrogel's mechanical and conductive properties for

pressure sensing. We will demonstrate that such an Au NWs/PAAm composite hydrogel can be in situ printed on electrodes to quickly fabricate high-performance wearable pressure sensors with good performances in terms of both sensitivity and operation range.

2. Results and Discussion

2.1. Micropatterning of Elastic Hydrogel

Figure 1a shows the scheme of photopolymerization process to form an elastic supramolecular hydrogel by using acrylamide (AAm) monomer and other components with UV light (details about the photopolymerization process are given in the experimental part). Although crosslinked PAAm hydrogels are usually fragile, their mechanical properties can be greatly improved after introducing secondary bonding forces.[13b, 14, 16] In our design, the AAm is photopolymerized with photoinitiator (Irgacure 2959) and crosslinked by the crosslinker (N,N-methylenebisacrylamide, MBA) to form a three-dimensional (3D) network through covalent bonds. Meanwhile, PAAm chains form a double-network hydrogel with poly(acrylic acid) (PAA) via hydrogen bonds. Moreover, PAA chains are simultaneously connected with Ca^{2+} by electrostatic force (ionic bond), which further enhances the mechanical strength of the PAAm composite hydrogel. Figure 1b illustrates the PAAm composite hydrogel under pressing. It can be recovered to the original shape after releasing the compression. Figure 1c shows the three kinds of bonds in the composite hydrogels, including covalent bonds, ionic bonds, and hydrogen bonds. The composite hydrogels own the elastic property after photo-annealing due to reversible breaking/bonding of ionic bonds and hydrogen bonds with and without pressure.[14, 16c] Figure S1 illustrates the elastic properties of the composite hydrogel with different photo-annealing times.

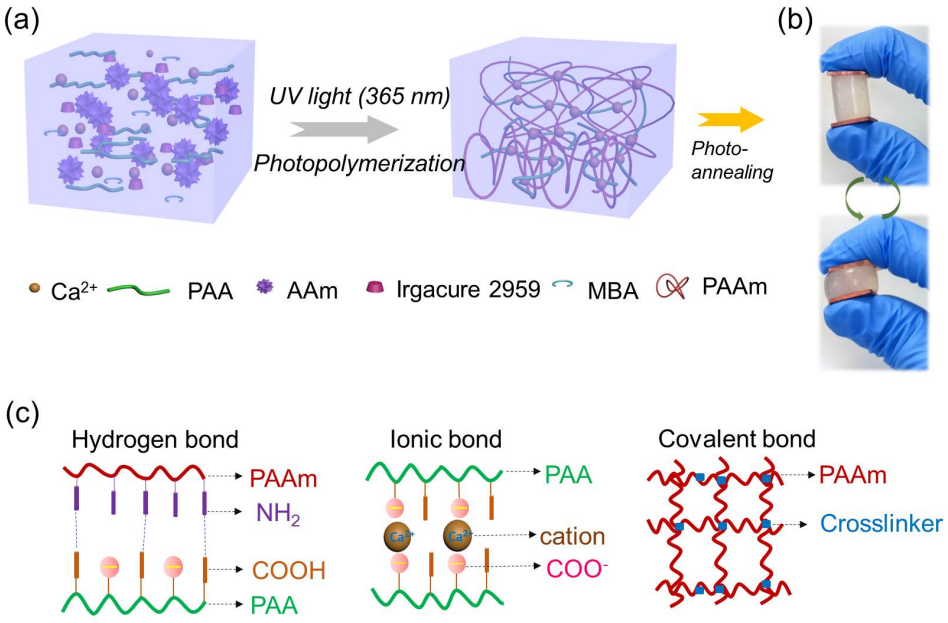

Figure 1. (a) Schemes of photopolymerization and crosslinking of AAm solution; (b) the shape changes of the elastic PAAm composite hydrogel under pressing or after releasing; (c) three kinds of bonds in the composite hydrogel: covalent bond between PAAm, hydrogen bond between PAAm and PAA, and ionic bond between PAA and Ca^{2+}.

The photocrosslinkable property of the solution makes the hydrogel printable via an optical maskless exposure technology for microstructure and device fabrication.[17] **Figure 2** illustrates the laser scanning confocal microscope images of the fabricated microstructures of the PAAm composite hydrogel. Figure 2a is a logo of The Hong Kong Polytechnic University (PolyU) and Figure 2b is a Chinese character which means best wishes and happiness. Figure 2c and 2d show arrays of micropillars and microtubes. All these microstructures were rapidly micropatterned by an in-house optical maskless exposure setup with a UV light source. The heights of all microstructures are around 105 μm (Figure S2). The remarkable height is attributed to the high photo-reactivity of AAm monomers and transparent properties of the composite hydrogel. The printable properties of PAAm composite hydrogels make them highly flexible for microdevice design and fabrication.

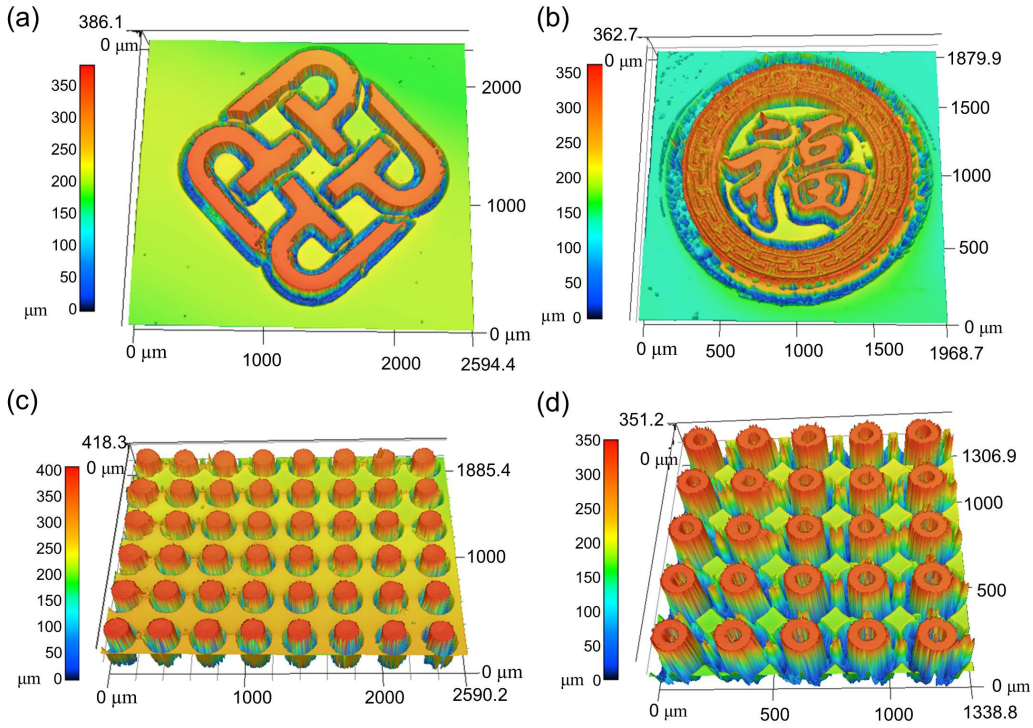

Figure 2. Laser scanning confocal images of the micropatterned PAAm composite hydrogel microstructures: (a) PolyU logo; (b) a Chinese character; (c) micropillars array; and (d) microtubes array.

2.2. Pressure Sensor Design and Working Mechanism

Scheme 1a shows the fabrication processes and working principle of the pressure sensor using PAAm composite hydrogel. AAm mixed solution was firstly dipped onto two electrodes. Then, an optical maskless exposure technology was applied to micropattern the hydrogel into micro-ribs on the target position. For such a photopolymerized composite hydrogel, crosslinked PAAm, PAA, and Ca^{2+} contribute to the elastic property, while Au NWs lead to the conductivity. Particularly, covalent crosslinked PAAm network plays an essential role in preserving the initial state of 3D hydrogel structure, while the dissociation/association of hydrogen bonds and ionic bonds are in favor of the energy dissipation,[14, 16c] and thus promote the elasticity of the composite hydrogel.

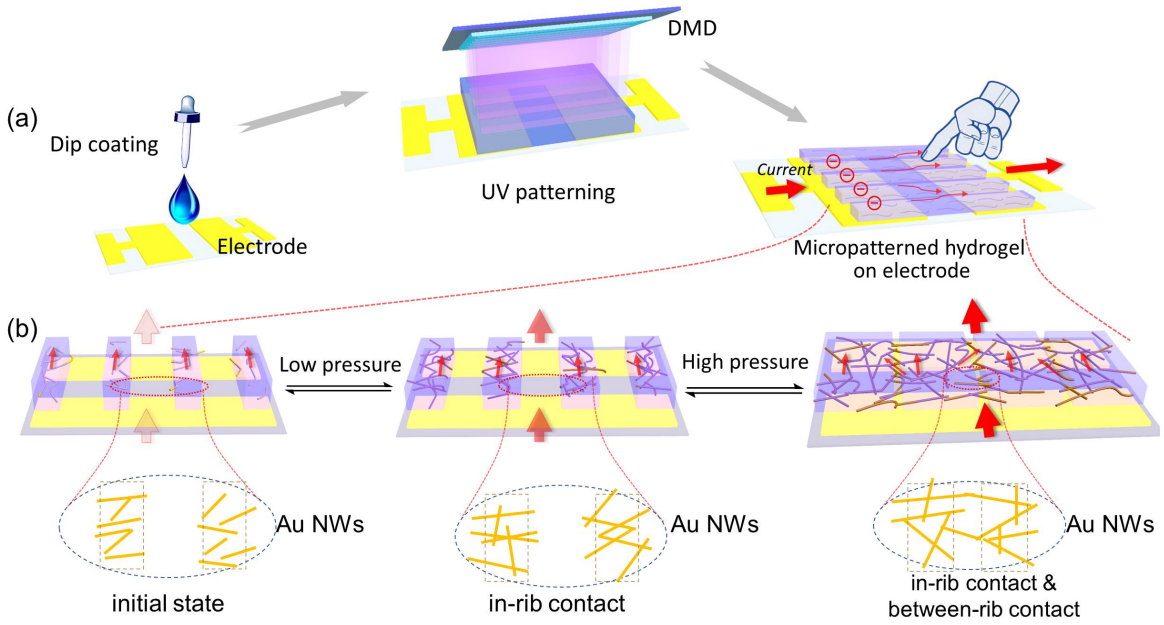

Scheme 1. Fabrication processes of the pressure sensor using PAAm composite hydrogel (a) and its working mechanism based on the bimodal contact mode of Au NWs (b).

The pressure sensing mechanism of the device is shown in Scheme 1b. Au NWs take crucial roles in the device: the pressure leads to tightly contact between Au NWs and thereby causes the increase of electrical current because of the reduction in the resistance of conductive hydrogels.[1c] Furthermore, the micro-rib structures make the device behave distinctly to bulk hydrogel-based pressure sensors.[18] When the micropatterned hydrogel is under relatively low pressure, the hydrogel elastically deforms with respect to the applied pressure where the voids between micro-ribs promote the hydrogel's elasticity and minimize the problems caused by viscoelastic behavior.[11a] If the hydrogel is further pressed, the induced change of deformation will becomes less significant due to the increased elastic resistance of the hydrogel materials as well as the structural interactions of the micro-ribs. A peculiar phenomenon arising from the micro-rib structure is that the pressure induced transverse expansion of micro-ribs will lead to the contact of Au NWs between adjacent micro-ribs and thereby cause an increase of current signal.[1c, 1e, 18] This between-rib contact mode provides a novel strategy to maneuver the sensitivity and operation range of the hydrogel-based pressure sensor.

2.3. Pressure Sensing Properties of Micropatterned Elastic Hydrogel

In the experiments, the pressure sensors with the micro-ribs of different widths ranging from 100 to 400 μm were fabricated and tested. The sensors with the micro-rib widths of 100, 200, 300, and 400 μm were labeled as sensor-1, sensor-2, sensor-3, and sensor-4, respectively. Another device without micro-rib structure, named as sensor-0, was fabricated for comparison. All sensors were photo-annealed with a UV lamp for 30 minutes to gain moderate elasticity (Figure S1). The widths and heights of the sensors are given in Figure S3. It can be seen the heights of devices are very close to each other in the range between 110 and 125 μm, which indicates the well-controlled fabrication process. The resistances of the five sensors increase with the widths of the gaps and micro-ribs (Figure S4), which can be ascribed to the reduction of Au NWs in the sensor when the gaps between micro-ribs become larger.

The sensors were tested by using a force gauge mounted on a stepping motor. The responses of the four pressure sensors with micro-ribs are shown in **Figure 3**. The sensitivities of sensor-1 and sensor-2 are 3.71 and 2.26 kPa^{-1} in the lower pressure ranges of 0-2.8 kPa and 0-2.6 kPa, respectively (Figure 3a and 3b). When the pressure is further increased, the sensitivities of the sensors decrease to 0.41 and 0.72 kPa^{-1}, respectively. However, the response curves of sensor-3 and sensor-4 show two deflection points (Figure 3c and 3d). Their sensitivities at the first stage are 2.44 and 2.73 kPa^{-1} in the pressure region of 0-1.3 and 0-0.9 kPa, respectively. Thereafter, they will drop to 0.31 and 0.23 kPa^{-1}, respectively. In surprise, their sensitivities will rise again to 0.65 and 0.69 kPa^{-1} when the applied pressures are increased to higher than 9 and 14 kPa, respectively. The sensitivity of these four sensors are much higher than that of sensor-0 which contains only bulk PAAm composite hydrogels (the sensitivity is 0.082 kPa^{-1} in the pressure region of 0-8 kPa, see Figure S5).

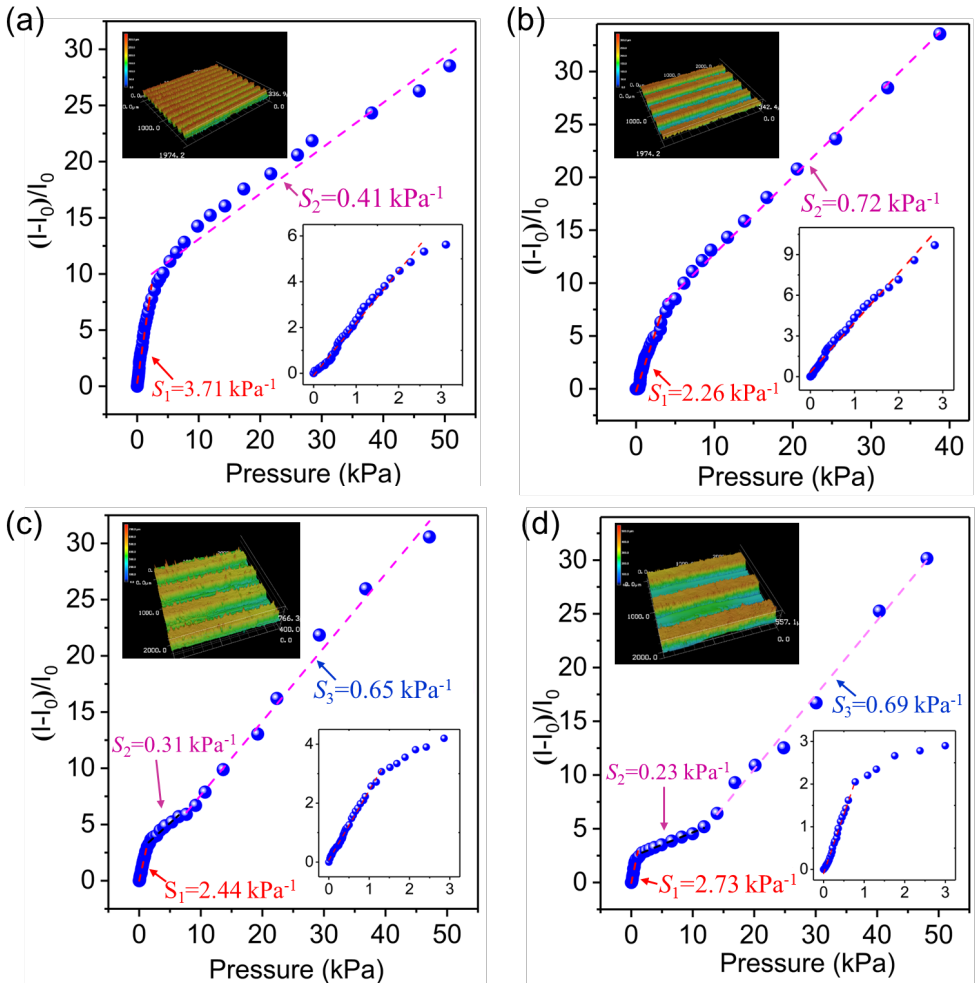

Figure 3. Current response and pressure sensitivities of the pressure sensors with the micro-ribs of different widths: (a) 100 μm, (b) 200 μm, (c) 300 μm, and (d) 400 μm. The left-upper insets show the microscopic images of micro-ribs, while the right-bottom insets are the enlarged graphs of the responses in the low-pressure range, i.e. 1-3 kPa.

Different from other pressure sensors whose sensitivities usually decrease with pressure,[1c-e, 1h, 8b, 11a, 13b] the sensitivities of sensor-3 and sensor-4 decrease first and then increase after reaching specific pressures. It is believed that such an extraordinary response originates from the unique between-rib contact mode of Au NWs (Scheme 1b) which can contribute extra electrical current with the increase of pressure. Evidently, the minimum pressure for squeezing the structure to achieve between-rib contact depends on the width of micro-ribs. Experimental results in Figure 3c and 3d agree well with the prediction, and the deflection point indicating the between-rib contact of sensor-3 is at 9 kPa which is lower than that of sensor-4, i.e. 14 kPa, because of the narrower width of the micro-ribs. From the

evolution of the deflection points in Figure 3, one can deduce that the between-rib contacts in sensor-1 and sensor-2 take place at very early stage. It is one reason why the sensitivity of sensor-1 in lower pressure regime is much higher than that of other piezoresistivity-type pressure sensors.[1c, 1e, 13]

2.4. Dynamic Response

Because of the high sensitivity and the wide linear-response range, sensor-1 was chosen to study in detail. Its dynamic response was measured by quick loading/unloading a pressure of 600 Pa for many cycles. The results are illustrated in **Figure 4**a, and the enlarged figure of a single cycle is shown in Figure 4b. It can be seen the rise time of the response from 0 to 600 Pa, called t_r, is 0.5 s, while the fall time of the response, called t_f, is 0.59 s. The response is relatively slow because of the viscoelastic property of the double-network hydrogel.[19] When the applied pressure is reduced to 11 Pa, the measured ratio of current change is about 0.01, as shown in Figure 4c. With the calculated noise level (i.e. 2.04×10^{-4}), it can be estimated that the device offers a low detection limit of 0.2 Pa at a signal-to-noise ratio of 3.

The long-term stability of the sensor was tested by loading/unloading for 10,000 cycles, as shown in Figure 4d. The pressure was increased gradually from 0 to 1 kPa for each cycle (7s for one cycle) rather than quick loading/unloading of a fixed force.[1c, 13a] No significant signal degradation was observed after 20-hour testing, which indicates the good durability of the sensor.

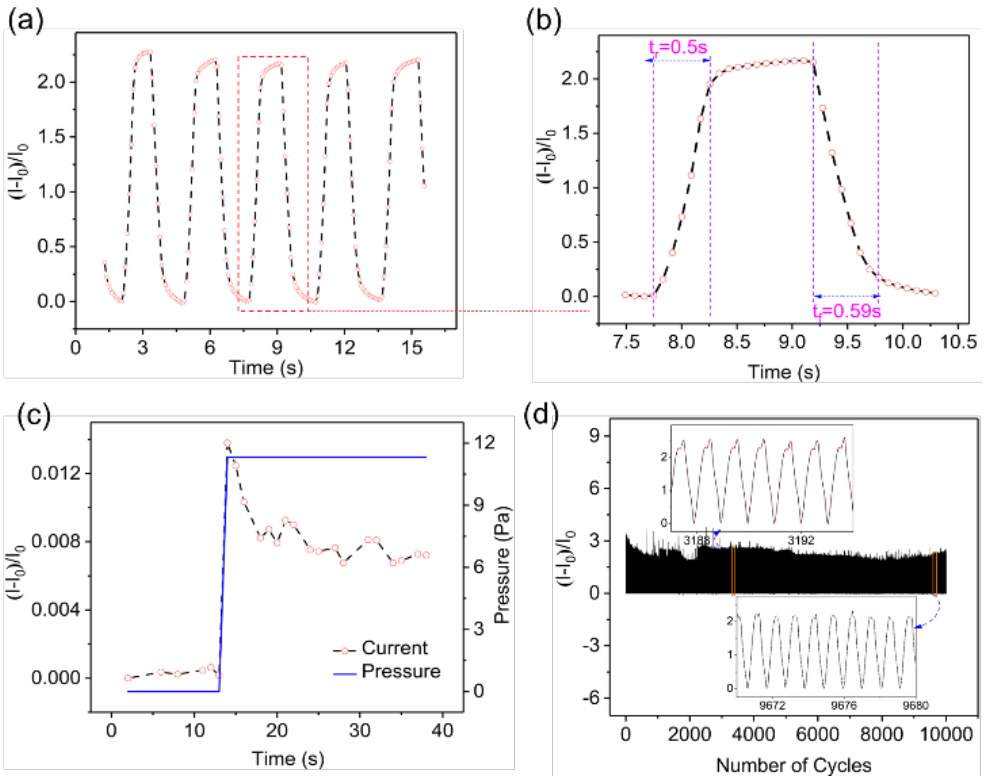

Figure 4. Dynamic response of sensor-1: (a) cycle test results; (b) enlarged response curve of one cycle; (c) detection limit; and (d) durability test for 20 hours (pressure change from 0 to 1 kPa). The inset shows the signals of two sections of the result.

2.5. Applications of Micropatterned Hydrogel Based Pressure Sensors

To demonstrate its easy deployment ability, the PAAm composite hydrogel was dipped and micropatterned on a flexible hand-shape electrode device (here we call it E-hand skin) for wearable pressure sensing, as shown in **Figure 5**a. In the experiments, 6 pressure sensors were fabricated on the electrodes of five fingers (the middle finger contains 2 sensors). Figure 5b shows the design of the E-hand skin, and Figure 5c illustrates the electric circuits for multiplexed signal collection. To facilitate multi-channel testing and measurement, the current-change induced voltage signals were measured to characterize the response of the sensor array in the E-skin hand. The E-hand skin can be easily attached on the soft-robot or gloves for tactile sensing applications. Figure 5d shows a glove, whose bottom surface is attached with the E-hand skin, for monitoring the pressing force of fingers when typing at the keyboard. Figure 5e shows the measured voltage change during the typing on a keyboard. As

expected, one signal was detected when one finger typed the keyboard, and more signals appeared when more fingers knocked the keyboard simultaneously. The amplitudes of the signals indicate the force of the fingers knocking the keyboard. The dynamic response clearly revealed the pressing and releasing time of the fingers during typing. Notably, all the six sensors worked very well, which indicates good working rate of the hydrogel-based pressure sensors.

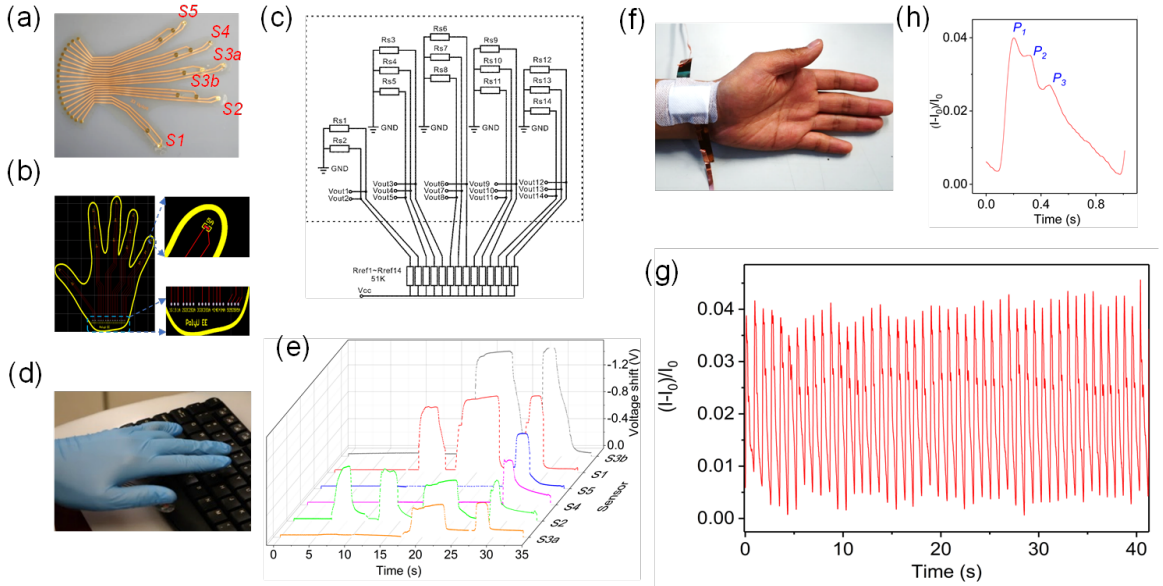

Figure 5. (a) Photo of the E-hand skin integrated with 6 pressure sensors; (b) electric design of the E-hand skin and (c) its electrical circuit; (d) a photo of a human hand worn with the E-hand skin for monitoring the pressing force during typing a keyboard and (e) the measured responses of the different sensors in the E-hand skin. (f) Photo of a human wrist banded with the composite hydrogel-based pressure sensor; (g) the measured pulse wave of radial artery pulses recorded for 40 s; and (h) the enlarged figure of a one-beat signal: three peaks were observed.

To demonstrate the potential applications of the pressure sensor for wearable applications, a PAAm composite-hydrogel pressure sensor was banded on the wrist to monitor arterial pulse wave, as shown in Figure 5f. Figure 5g shows the real-time measurement of wrist pulse for about 40 s. The pulse rate could be directly read out as 70 beats/min. An enlarged image of a single-pulse wave is shown in Figure 5h. One can see that three obviously distinguishable peaks, which are known as the superposition of the incoming blood wave ejected by the left ventricular and the reflected wave from the lower body,[20] are observed.

The calculated radial augmentation index, $AI_r=P_2/P_1$, which is a characteristic value for arterial stiffness and highly related to the age of people, from the measured waveform is around 0.72. The result agrees well with the data for a 32-years-old male.[20] The time delay between the first and second peaks, $\Delta T_{DVP}=t_{P2}-t_{P1}$, which is another indicator of health, are determined to be ~120 ms. Moreover, the result also reveals some small features in the diastolic tails of the pulse pressure waves, which are hard to be measured by most of wearable sensors in existing arterial tonometry.

In general, supramolecular hydrogels have great potential for artificial skin-like devices fabrication because of their unique tunability in both mechanical and sensory properties.[16a, 16c] Taking advantages of their excellent stretchability, the PAAm hydrogels have been applied in many fields, including stretchable hydrogel circuit boards,[21] ionic conductors,[15a] electroluminescent skin for tactile sensing,[22] and ionic touch panel.[23] The novel supramolecular hydrogel system of this work was designed by crosslinking PAAm through covalent bonds and simultaneously forming dynamic bonds, i.e. hydrogen bonds and ionic bonds, with PAA and Ca^{2+}. The results in Figure S1 indicate that the elastic property of the supramolecular hydrogel system can be flexibly tuned by photo-annealing process. It can be attributed to the tunable crosslinking degree of the hydrogel, whose PAAm chains can be further crosslinked by photon energy.[24]

It is noteworthy that the micro-rib structure provides an extra strategy to tune the response curve of the hydrogel-based pressure sensor because of the bimodal contact mechanism, i.e. inner-rib and between-rib contacts of Au NWs. As shown in Figure 3, the between-rib contact mode depends very much on the width of micro-ribs. It means that one can optimize the sensitivity or even operation range of the sensor through tailoring the width of micro-ribs. Indeed, the high sensitivity of sensor-1 are believed to result from both inner-rib and between-rib contact of Au NWs. As shown in Table S1, the sensitivity of sensor-1 is

about ten times higher than that of other PAAm-based piezoresistivity-type pressure sensor.[13b] Moreover, as shown in Figure S5, the responsive range of the pressure sensors with micro-ribs can be as wide as 0–50 kPa, while the response of the sensor without micro-rib structure (i.e. sensor-0) got saturated when the pressure reached 8 kPa. Compared with previously reported piezoresistivity-type pressure sensors,[1d, 1e, 1h, 13a] our sensors have much wider responsive range (varying from several times to tens of times) while still have high sensitivity.

3. Conclusion

In conclusion, a photocrosslinkable supramolecular hydrogel using AAm monomer, PAA, and Ca^{2+} aqueous solution has been developed to prepare highly elastic composite hydrogel via photopolymerization. Au NWs were mixed into the PAAm hydrogel to make the composite hydrogel conductive under direct voltage. An optical maskless exposure technology has been applied to precisely pattern the composite hydrogel into micro-rib structures and control its crosslinking degree to tune the mechanical property simultaneously. The fabricated pressure sensors with micro-rib structures revealed a bimodal contact mode of Au NWs which can be exerted to tailor the sensitivity and operation range. Such a supramolecular hydrogel can be rapidly printed on flexible substrates to fabricate low-cost high-performance pressure sensors, which thus has a wide variety of promising applications ranging from wearable healthcare devices to soft robots.

4. Experimental Section

Materials: Acrylamide, N,N-methylenebisacrylamide (MBA), 2-hydroxy-4′-(2-hydroxyethoxy)-2-methylpropiophenone (Irgacure 2959), and poly (acrylic acid) (PAA, Mw = 100 000 g mol^{-1}, 35 wt% aqueous solution) were purchased from Sigma-Aldrich. Gold nanowires (Au NWs) were purchased from Nanjing XFNANO Materials Tech Co., Ltd.

$CaCl_2$ and ethanol were analytical grade. Deionized (DI) water with a resistance of 18 MΩ cm was used in all experiments.

Micropatterning of PAAm Composite Hydrogels: 1.8 g of acrylamide monomer was dissolved in 2.3 g of DI water. Then, 0.26 g of PAA, 0.1 g of Irgacure 2959 (photoinitiator), 0.0072 g of MBA (crosslinker), and 0.0125 g of $CaCl_2$ were added stepwise until fully dissolved under stirring. The prepared photoresist solution was stored for use.

Au NWs with a diameter of 3 nm and a length of 0.9–10 μm were homogenously dispersed into isopropanol solvent to prepare a solution of 20 mg/mL. The Au NWs solution (0.1 g) was then mixed into the above-prepared aqueous solution (0.9 g) under stirring.

An in-house optical maskless exposure setup was used for micropatterning process. The above-prepared photoresist solution was dropped upon a glass slide and then covered by a cover glass. The pre-designed micropatterns were then converted into image data and loaded onto the digital-mirror device for optical exposure process. UV light source (365 nm) was used for photopolymerization of photoresist solutions. The intensity of UV light was 14.97 mW/cm^2. The total exposure time was 10–30 s. The exposed micropatterns were developed by ethanol and DI water, sequentially.

Device Fabrication: Flexible copper films were used to prepare the electrodes, whose interval was kept as 200 μm. The prepared photoresist solution was dropped onto the electrodes. Then, the photoresist solution was irradiated by the UV light with the designed micro-rib patterns. The intensity of the UV light was 14.97 mW/cm^2, and the exposure time was 15 s. After patterning process, they were photo-annealed by an 8W-UV light for 30 minutes to reach desired elasticity. Finally, the device was packaged by using a thin polyethylene film.

Characterizations and Device Tests: Microstructures of PAAm composite hydrogels were measured by 3D laser scanning confocal microscope (VK-X200, KEYENCE, Japan). It is a non-contact laser scanning imaging machine. The magnification of objective lens used for scanning was 50×.

The responses of the pressure sensors were tested by Keithley 2400 Source Meter (1V voltage was provided to measure the devices), while the multi-channel testing of E-skin hand was carried out by using a data acquisition card (National Instruments USB-6216 Data Acquisition Card). The force applied on the sensors was precisely controlled with a force gauge (MODELNO: JSV-H1000). The response data were real-time recorded by using a LabVIEW software.

For the LED switch tests, the voltage was supplied with a 10-V source. The sensor was connected to a LED in series, and the force was applied with the force gauge.

Supporting Information

Supporting Information is available from the Wiley Online Library or from the author.

Acknowledgements

This work was partially supported by NSFC/RGC Joint Research Scheme (Grant No.: N_PolyU517/15) and PolyU Departmental General Research Fund (Project Code: 1-ZVHB), and partially supported by the National Natural Science Foundation of China (No.: 51561165011). M.J.Y thanks for Dr. Zhengyong Liu's help on writing LabVIEW programs for testing of the devices.

Conflict of Interest

The authors declare no conflict of interest.

Received: ((will be filled in by the editorial staff))
Revised: ((will be filled in by the editorial staff))
Published online: ((will be filled in by the editorial staff))

References

[1] (a) T. Someya, Y. Kato, T. Sekitani, S. Iba, Y. Noguchi, Y. Murase, H. Kawaguchi, T. Sakurai, *Proc. Natl. Acad. Sci. U.S.A.* **2005,** *102,* 12321; (b) G. Schwartz, B.C.K. Tee, J.

Mei, A.L. Appleton, D.H. Kim, H. Wang, Z. Bao, *Nat. Commun.* **2013,** *4,* 1859; (c) S. Gong, W. Schwalb, Y.W. Wang, Y. Chen, Y. Tang, J. Si, B. Shirinzadeh, W.L. Cheng, *Nat. Commun.* **2014,** *5,* 3132; (d) L. Pan, A. Chortos, G. Yu, Y. Wang, S. Isaacson, R. Allen, Y. Shi, R. Dauskardt, Z. Bao, *Nat. Commun.* **2014,** *5,* 3002; (e) H. Park, Y.R. Jeong, J. Yun, S.Y. Hong, S. Jin, S.-J. Lee, G. Zi, J.S. Ha, *ACS Nano* **2015,** *9,* 9974; (f) Y. Zang, F. Zhang, D. Huang, X. Gao, C.-a. Di, D. Zhu, *Nat. Commun.* **2015,** *6,* 6269; (g) K.-Y. Chun, Y.J. Son, C.-S. Han, *ACS Nano* **2016,** *10,* 4550; (h) D. Lee, H. Lee, Y. Jeong, Y. Ahn, G. Nam, Y. Lee, *Adv. Mater.* **2016,** *28,* 9364.

[2] (a) F. Güder, A. Ainla, J. Redston, B. Mosadegh, A. Glavan, T.J. Martin, G.M. Whitesides, *Angew. Chem. Int. Ed.* **2016,** *55,* 5727; (b) H. Guo, C. Lan, Z. Zhou, P. Sun, D. Wei, C. Li, *Nanoscale* **2017,** *9,* 6246.

[3] (a) C. Pang, G.-Y. Lee, T.-i. Kim, S.M. Kim, H.N. Kim, S.-H. Ahn, K.-Y. Suh, *Nat. Mater.* **2012,** *11,* 795; (b) A.P. Gerratt, H.O. Michaud, S.P. Lacour, *Adv. Funct. Mater.* **2015,** *25,* 2287.

[4] (a) L. Sambe, V.R. de La Rosa, K. Belal, F. Stoffelbach, J. Lyskawa, F. Delattre, M. Bria, G. Cooke, R. Hoogenboom, P. Woisel, *Angew. Chem. Int. Ed.* **2014,** *53,* 5044; (b) X. Ren, K. Pei, B. Peng, Z. Zhang, Z. Wang, X. Wang, P.K.L. Chan, *Adv. Mater.* **2016,** *28,* 4832.

[5] (a) M.L. Hammock, A. Chortos, B.C.K. Tee, J.B.H. Tok, Z. Bao, *Adv. Mater.* **2013,** *25,* 5997; (b) A. Chortos, J. Liu, Z. Bao, *Nat. Mater.* **2016,** *15,* 937.

[6] (a) D.-H. Kim, N. Lu, R. Ma, Y.-S. Kim, R.-H. Kim, S. Wang, J. Wu, S.M. Won, H. Tao, A. Islam, K.J. Yu, T.-i. Kim, R. Chowdhury, M. Ying, L. Xu, M. Li, H.-J. Chung, H. Keum, M. McCormick, P. Liu, Y.-W. Zhang, F.G. Omenetto, Y. Huang, T. Coleman, J.A. Rogers, *Science* **2011,** *333,* 838; (b) R. Feiner, L. Engel, S. Fleischer, M. Malki, I. Gal, A. Shapira, Y. Shacham-Diamand, T. Dvir, *Nat. Mater.* **2016,** *15,* 679; (c) S.-K. Kang, R.K.J. Murphy, S.-W. Hwang, S.M. Lee, D.V. Harburg, N.A. Krueger, J. Shin, P.

Gamble, H. Cheng, S. Yu, Z. Liu, J.G. McCall, M. Stephen, H. Ying, J. Kim, G. Park, R.C. Webb, C.H. Lee, S. Chung, D.S. Wie, A.D. Gujar, B. Vemulapalli, A.H. Kim, K.-M. Lee, J. Cheng, Y. Huang, S.H. Lee, P.V. Braun, W.Z. Ray, J.A. Rogers, *Nature* **2016,** *530,* 71.

[7] (a) B.C.K. Tee, C. Wang, R. Allen, Z. Bao, *Nat. Nano.* **2012,** *7,* 825; (b) Z.L. Wang, W. Wu, *Angew. Chem. Int. Ed.* **2012,** *51,* 11700; (c) Y. Zang, F. Zhang, C.-a. Di, D. Zhu, *Mater. Horiz.* **2015,** *2,* 140.

[8] (a) H.M. Lee, S.-Y. Choi, A. Jung, S.H. Ko, *Angew. Chem. Int. Ed.* **2013,** *52,* 7718; (b) D. Kwon, T.-I. Lee, J. Shim, S. Ryu, M.S. Kim, S. Kim, T.-S. Kim, I. Park, *ACS Appl. Mater. Inter.* **2016,** *8,* 16922.

[9] M. Kaltenbrunner, T. Sekitani, J. Reeder, T. Yokota, K. Kuribara, T. Tokuhara, M. Drack, R. Schwodiauer, I. Graz, S. Bauer-Gogonea, S. Bauer, T. Someya, *Nature* **2013,** *499,* 458.

[10] (a) C. Pan, L. Dong, G. Zhu, S. Niu, R. Yu, Q. Yang, Y. Liu, Z.L. Wang, *Nat. Photon.* **2013,** *7,* 752; (b) W. Wu, X. Wen, Z.L. Wang, *Science* **2013,** *340,* 952; (c) H.-B. Yao, J. Ge, C.-F. Wang, X. Wang, W. Hu, Z.-J. Zheng, Y. Ni, S.-H. Yu, *Adv. Mater.* **2013,** *25,* 6692.

[11] (a) S.C.B. Mannsfeld, B.C.K. Tee, R.M. Stoltenberg, C.V.H.H. Chen, S. Barman, B.V.O. Muir, A.N. Sokolov, C. Reese, Z. Bao, *Nat. Mater.* **2010,** *9,* 859; (b) D.J. Lipomi, M. Vosgueritchian, B.C.K. Tee, S.L. Hellstrom, J.A. Lee, C.H. Fox, Z. Bao, *Nat. Nano.* **2011,** *6,* 788.

[12] L. Lin, Y. Xie, S. Wang, W. Wu, S. Niu, X. Wen, Z.L. Wang, *ACS Nano* **2013,** *7,* 8266.

[13] (a) Y. Tai, M. Mulle, I. Aguilar Ventura, G. Lubineau, *Nanoscale* **2015,** *7,* 14766; (b) J. Duan, X. Liang, J. Guo, K. Zhu, L. Zhang, *Adv. Mater.* **2016,** *28,* 8037.

[14] J.-Y. Sun, X. Zhao, W.R.K. Illeperuma, O. Chaudhuri, K.H. Oh, D.J. Mooney, J.J. Vlassak, Z. Suo, *Nature* **2012,** *489,* 133.

[15] (a) C. Keplinger, J.-Y. Sun, C.C. Foo, P. Rothemund, G.M. Whitesides, Z. Suo, *Science* **2013,** *341,* 984; (b) N.N. Jason, M.D. Ho, W. Cheng, *J. Mater. Chem. C* **2017,** *5,* 5845; (c) S. Gong, W. Cheng, *Adv. Electro. Mater.* **2017,** *3,* 1600314.

[16] (a) S. Sun, L.-B. Mao, Z. Lei, S.-H. Yu, H. Cölfen, *Angew. Chem. Int. Ed.* **2016,** *55,* 11765; (b) W. Sun, B. Xue, Y. Li, M. Qin, J. Wu, K. Lu, J. Wu, Y. Cao, Q. Jiang, W. Wang, *Adv. Funct. Mater.* **2016,** *26,* 9044; (c) J. Liu, C.S.Y. Tan, Z. Yu, N. Li, C. Abell, O.A. Scherman, *Adv. Mater.* **2017,** *29,* 1605325.

[17] M.-J. Yin, M. Yao, S. Gao, A.P. Zhang, H.-Y. Tam, P.-K.A. Wai, *Adv. Mater.* **2016,** *28,* 1394.

[18] Y. Lu, J.Y. Huang, C. Wang, S. Sun, J. Lou, *Nat. Nano.* **2010,** *5,* 218.

[19] Y. Mao, S. Lin, X. Zhao, L. Anand, *J. Mech. Phys. Solids* **2017,** *100,* 103.

[20] W.W. Nichols, *Am. J. Hypertens.* **2005,** *18,* 3S.

[21] H. Yuk, T. Zhang, G.A. Parada, X. Liu, X. Zhao, *Nat. Commun.* **2016,** *7*.

[22] C. Larson, B. Peele, S. Li, S. Robinson, M. Totaro, L. Beccai, B. Mazzolai, R. Shepherd, *Science* **2016,** *351,* 1071.

[23] C.-C. Kim, H.-H. Lee, K.H. Oh, J.-Y. Sun, *Science* **2016,** *353,* 682.

[24] E. Andrzejewska, *Prog. Polym. Sci.* **2001,** *26,* 605.

Supporting Information

Micropatterned Elastic Gold-Nanowire/Polyacrylamide Composite Hydrogels for Wearable Pressure Sensors

*Ming-jie Yin [a], Yangxi Zhang [a], Zhigang Yin [b], Qingdong Zheng [b], and A. Ping Zhang [a,]**

[a] Photonics Research Center, Department of Electrical Engineering, The Hong Kong Polytechnic University, Hong Kong SAR, China

[b] State Key Laboratory of Structural Chemistry, Fujian Institute of Research on the Structure of Matter, Chinese Academy of Sciences, 155 Yangqiao West Road, Fuzhou, China.

*E-mail: azhang@polyu.edu.hk

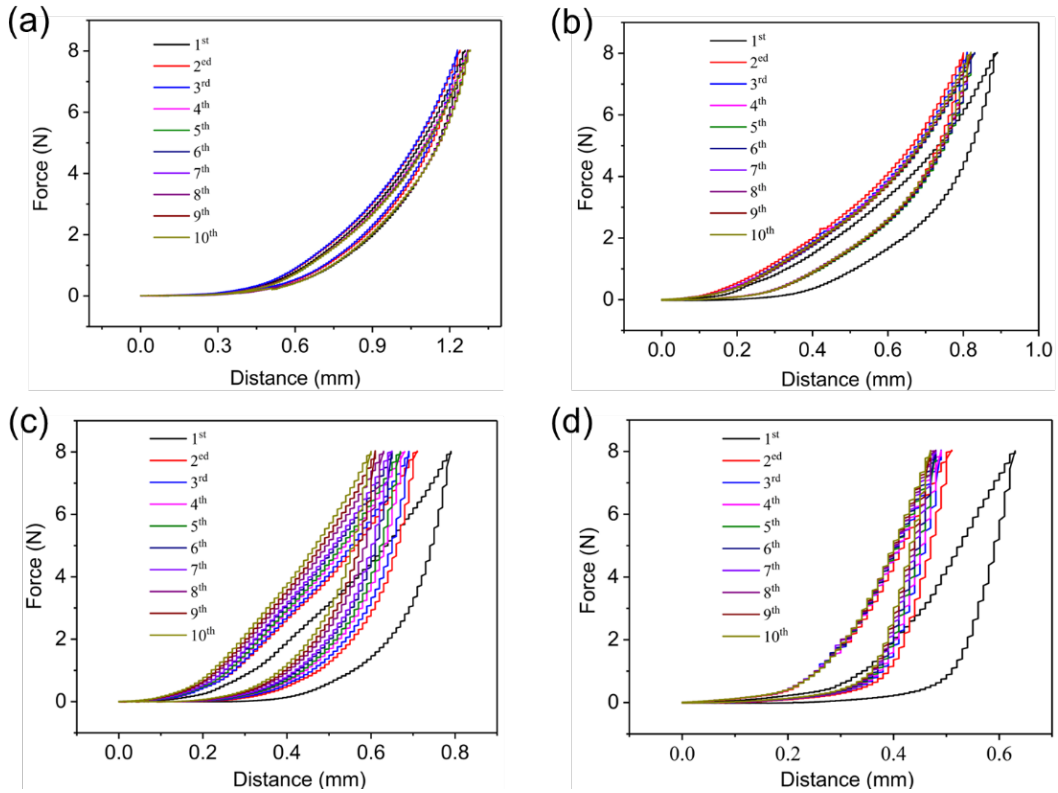

Figure S1. Elastic properties of the PAAm composite hydrogel photo-annealed with different time: (a) 15 minutes; (b) 30 minutes; (c) 45 minutes; and (d) 60 minutes.

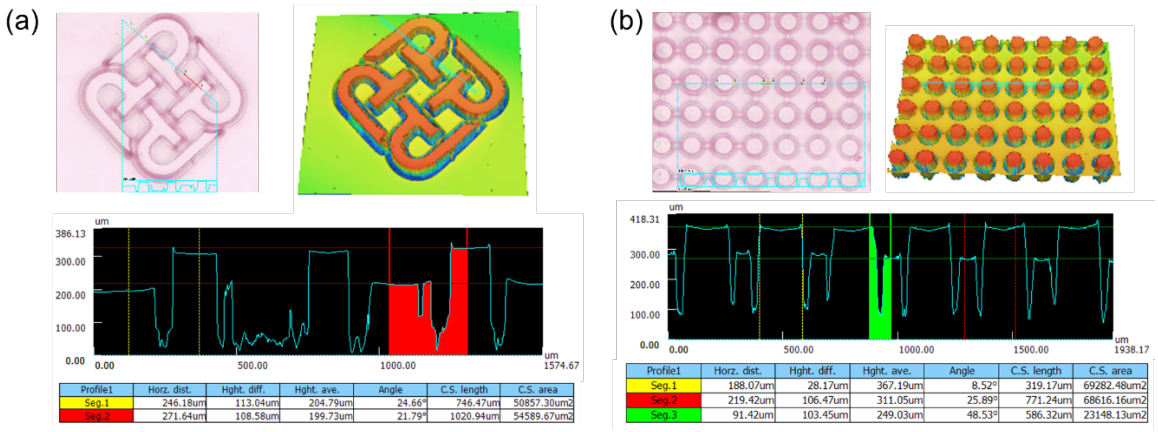

Profile1	Horz. dist.	Hght. diff.	Hght. ave.	Angle	C.S. length	C.S. area
Seg.1	246.18um	113.04um	204.79um	24.66°	746.47um	50857.30um2
Seg.2	271.64um	108.58um	199.73um	21.79°	1020.94um	54589.67um2

Profile1	Horz. dist.	Hght. diff.	Hght. ave.	Angle	C.S. length	C.S. area
Seg.1	188.07um	28.17um	367.19um	8.52°	319.17um	69282.48um2
Seg.2	219.42um	106.47um	311.05um	25.89°	771.24um	68616.16um2
Seg.3	91.42um	103.45um	249.03um	48.53°	586.32um	23148.13um2

Figure S2. Measured geometric parameters of the fabricated PAAm composite hydrogel microstructures: (a) logo of PolyU; (b) micropillars array.

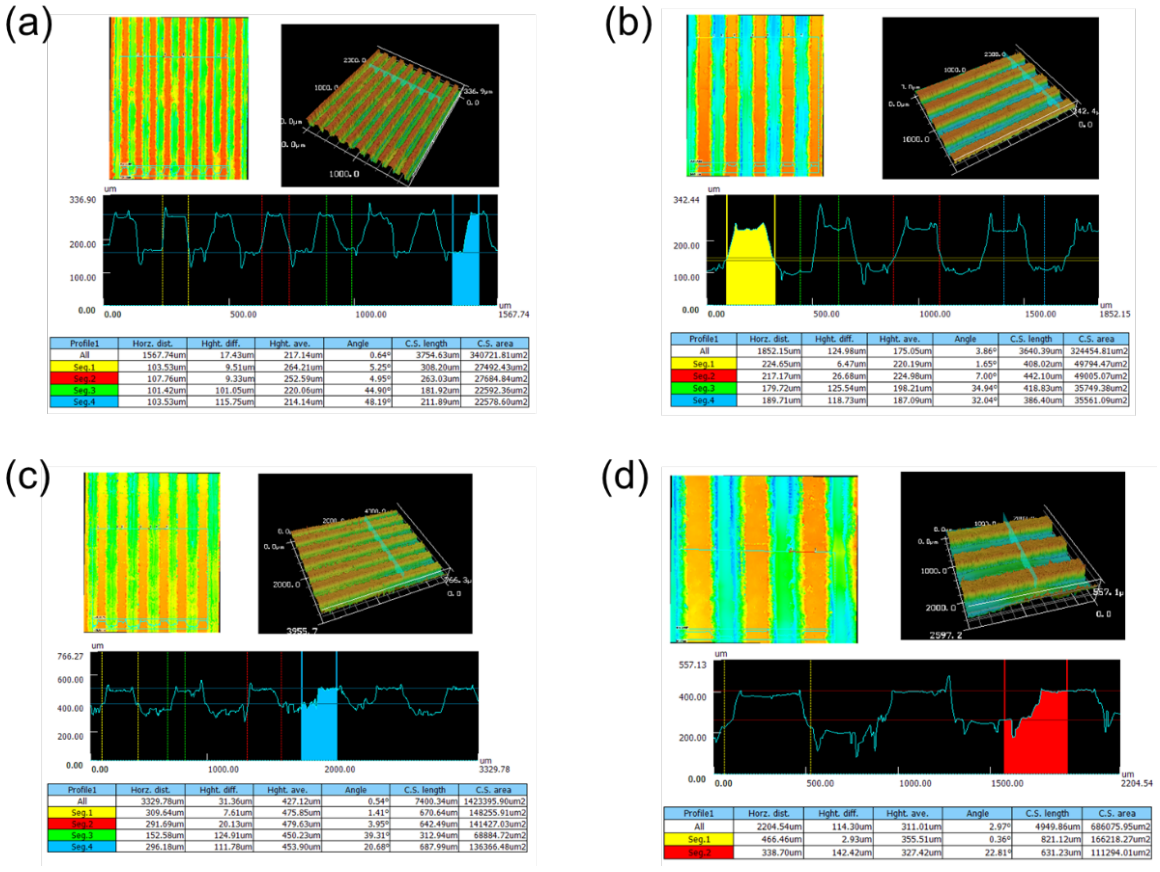

Profile1	Horz. dist.	Hght. diff.	Hght. ave.	Angle	C.S. length	C.S. area
All	1567.74um	17.43um	217.14um	0.64°	3754.63um	340721.81um2
Seg.1	103.53um	9.51um	264.21um	5.25°	308.20um	27492.43um2
Seg.2	107.76um	9.33um	252.59um	4.95°	263.03um	27684.84um2
Seg.3	101.42um	101.05um	220.06um	44.90°	181.92um	22592.36um2
Seg.4	103.53um	115.75um	214.14um	48.19°	211.89um	22578.60um2

Profile1	Horz. dist.	Hght. diff.	Hght. ave.	Angle	C.S. length	C.S. area
All	1852.15um	124.98um	175.05um	3.86°	3640.39um	324454.81um2
Seg.1	224.65um	6.47um	220.19um	1.65°	468.02um	49794.47um2
Seg.2	217.17um	26.68um	224.98um	7.00°	442.10um	49805.07um2
Seg.3	179.72um	125.54um	198.21um	34.94°	418.83um	35749.38um2
Seg.4	189.71um	118.73um	187.09um	32.04°	386.40um	35561.09um2

Profile1	Horz. dist.	Hght. diff.	Hght. ave.	Angle	C.S. length	C.S. area
All	3329.78um	31.36um	427.12um	0.54°	7400.34um	1423395.90um2
Seg.1	309.64um	7.61um	475.85um	1.41°	670.64um	148255.91um2
Seg.2	291.69um	20.13um	479.63um	3.95°	642.49um	141427.03um2
Seg.3	152.58um	124.91um	450.23um	39.31°	312.94um	68884.72um2
Seg.4	296.18um	111.78um	453.90um	20.68°	687.99um	136366.48um2

Profile1	Horz. dist.	Hght. diff.	Hght. ave.	Angle	C.S. length	C.S. area
All	2204.54um	114.30um	311.01um	2.97°	4949.86um	686075.95um2
Seg.1	466.46um	2.93um	355.51um	0.36°	821.12um	166218.27um2
Seg.2	338.70um	142.42um	327.42um	22.81°	631.23um	111294.01um2

Figure S3. Measured geometric parameters of the micro-ribs for the devices. (a) 100-μm micro-ribs: the lateral width is 105 μm and the height is 110 μm; (b) 200-μm micro-ribs: the lateral width is 220 μm and the height is 120 μm; (c) 300-μm micro-ribs: the lateral width is 300 μm and the height is 115 μm; and (d) 400-μm micro-ribs: the lateral width is 450 μm and the height is 125 μm.

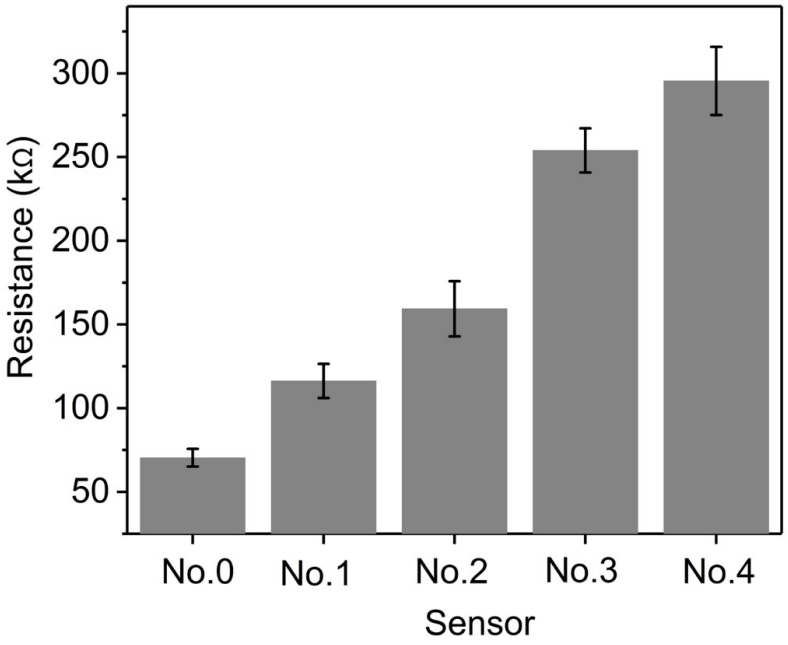

Figure S4. Initial resistance of the five sensors with different micro-rib widths (the area of each sensor is 4 cm^2, while the gap areas of the sensors from No. 0 to No. 4 are 0, 1.2, 1.5, 2, and 2.25 cm2, respectively), the error bar is also provided based on the average value of four devices prepared at the same condition.

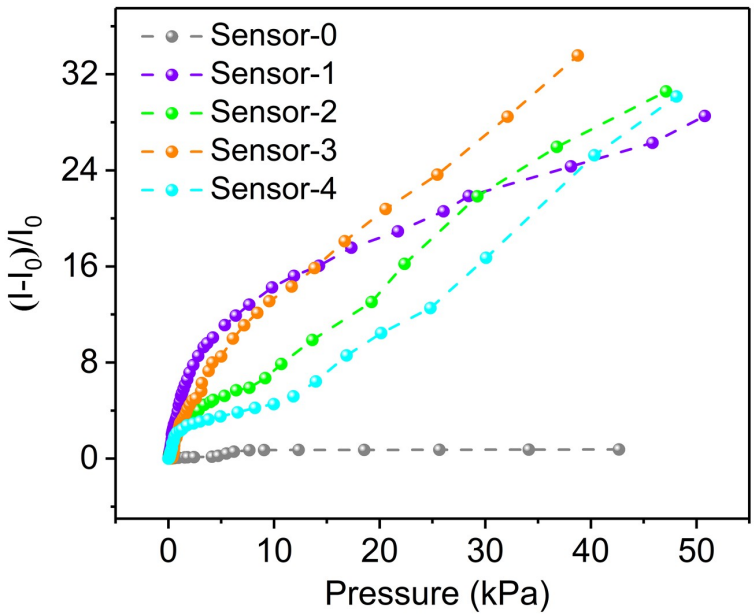

Figure S5. Comparison of the responses of the five sensors without (sensor-0) and with (sensor-1, sensor-2, sensor-3, and sensor-4) patterning of the micro-rid structures.

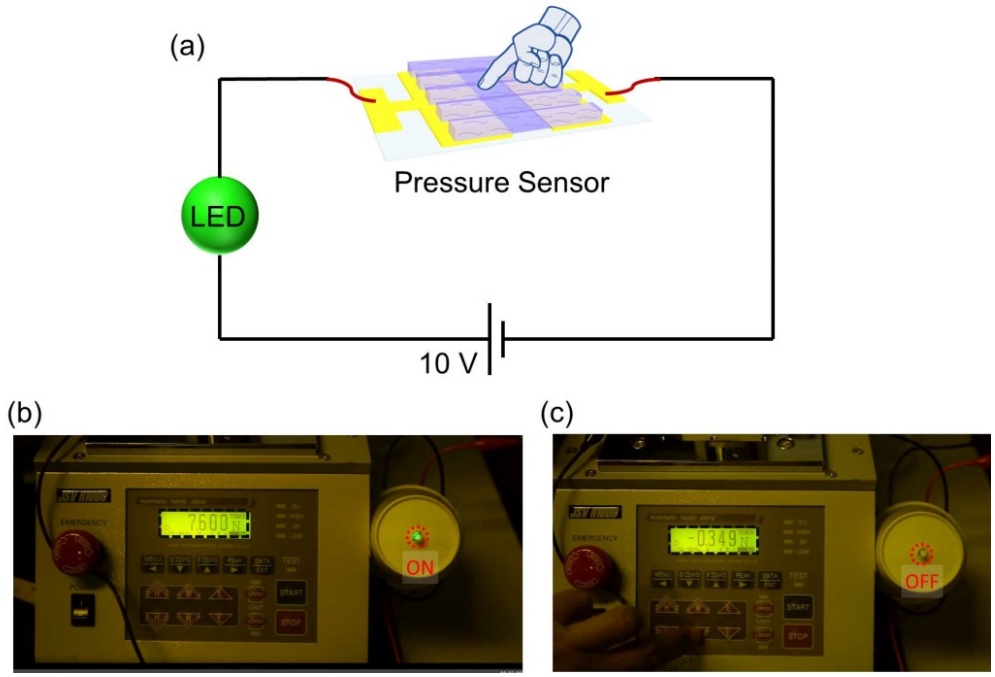

Figure S6. Demonstration of a pressure-control switch using the composite hydrogel-based pressure sensor: (a) the electrical circuit for testing; (b, c) The light emitting diode was switched on/off by pressing/releasing the pressure sensor.

Table S1 Comparison of the present pressure sensor with previously reported elastic polymer-based sensors.

Types of Devices	Elastic Materials	Operation Range (kPa)	Sensitivity (kPa^{-1})	Working Voltage	Ref
Piezoresistivity (patterned)	PDMS+PANi	0-0.22 0.22-1 1-3.5	2 0.87 0.12	V_{ds}= 1 V	1
Piezoresistivity (no pattern)	PDMS+Au NWs	0-5	1.14	V_{ds}= 1.5 V	2
Piezoresistivity (no pattern)	PDMS+SWNTs	0-0.3 0.3-1.2	1.8 0.11	V_{ds}= 2 V	3
Piezoresistivity (no pattern)	PU+RGO	0-2 2-10	0.26 0.03	———	4
Piezoresistivity (no pattern)	PU+SSNPs	0-1 1-8.2 10-18	2.46 0.52 0.055	V_{ds}= 1 V	5
Piezoresistivity (patterned)	PPy	0-0.03 0.03-0.1 1-10	133 41.9-7.7 0.4-0.05	———	6
Piezoresistivity (no pattern)	PAAm+CSM+ PANi	0-1 1-10	0.35 0.05	———	7
Piezoresistivity (patterned)	PAAm+PAA+ Au NWs	0-2.5 2.5-50	3.71 0.41	V_{ds}= 1 V	This work

[1] H. Park, Y.R. Jeong, J. Yun, S.Y. Hong, S. Jin, S.-J. Lee, G. Zi, J.S. Ha, *ACS Nano* **2015,** *9,* 9974.
[2] S. Gong, W. Schwalb, Y.W. Wang, Y. Chen, Y. Tang, J. Si, B. Shirinzadeh, W.L. Cheng, *Nat. Commun.* **2014,** *5,* 3132.
[3] X. Wang, Y. Gu, Z. Xiong, Z. Cui, T. Zhang, *Adv. Mater.* **2014,** *26,* 1336.
[4] H.-B. Yao, J. Ge, C.-F. Wang, X. Wang, W. Hu, Z.-J. Zheng, Y. Ni, S.-H. Yu, *Adv. Mater.* **2013,** *25,* 6692.
[5] D. Lee, H. Lee, Y. Jeong, Y. Ahn, G. Nam, Y. Lee, *Adv. Mater.* **2016,** *28,* 9364.
[6] L. Pan, A. Chortos, G. Yu, Y. Wang, S. Isaacson, R. Allen, Y. Shi, R. Dauskardt, Z. Bao, *Nat. Commun.* **2014,** *5,* 3002.
[7] J. Duan, X. Liang, J. Guo, K. Zhu, L. Zhang, *Adv. Mater.* **2016,** *28,* 8037.